



Sol–gel approach for the growth of vertically aligned 3D-TiO₂ nanorod arrays as an efficient photoanode for high-performance dye-sensitized solar cells

Zhila Khakpour¹ · Mohaddeseh Tavassoli¹ · Omran Moradlou¹

Received: 9 May 2019 / Accepted: 3 December 2019 / Published online: 10 December 2019
© Iranian Chemical Society 2019

Abstract

In this study, a facile, low cost, and scalable sol–gel method has been proposed for the coating of ultra-thin layer of TiO₂ on FTO substrate as a seed layer for the growth of 3D-TiO₂ nanorod (3D-TiO₂-NR) arrays on FTO. Then, the two-step hydrothermal process including nanorod growth and the chemical etching treatment was proceeded for the fabrication of FTO/3D-TiO₂-NR photoanodes. The thickness of the deposited TiO₂ in FTO/TiO₂-sg samples was measured with small-angle X-ray scattering technique, and it was obtained to be 21.3 nm. FE-SEM and TEM techniques were used for the morphological characterization of 3D-TiO₂-NR, and it was obtained that the tightly adhered film of vertically aligned 3D-TiO₂-NR with two-layer nanostructuring is formed with a cubic base and a nanorods head. Finally, DSSCs with iodine-based and cobalt(II/III) tris(2,2'-bipyridine) complex-based electrolytes with two different photoanodes including 3D-TiO₂-NR and TiO₂-NP were assembled and their photovoltaic characteristics were investigated. For [Co(bpy)₃]^{2+/3+} shuttle-based DSSC, the obtained power conversion efficiency (η) was about 3.5% with J_{sc} of 9.36 mA cm⁻² in 3D-TiO₂-NR-based DSSC, while η of TiO₂-NP-based DSSC was about 1.4%. The results showed that employing 3D-TiO₂-NR-based photoanode in DSSCs with bulky electron shuttles remarkably improves the photovoltaic characteristics of DSSCs. Electrochemical impedance spectroscopic studies also showed the lower charge transfer resistances for DSSCs with nanorod-based photoanode building blocks.

Keywords DSSC · TiO₂ nanorod arrays · Electron shuttle · Adhesion · Sol–gel · Cobalt(II/III) tris(2,2'-bipyridine) complexes

Introduction

With the strong demand in green and renewable energies, solar energy is attracting global attention [1–3]. Among various renewable energies such as biomass, hydrogen energy, and wind energy, solar energy is one of the most popular sustainable energy resources which is achievable by using photovoltaic and photoelectrochemical cells [4, 5]. Dye-sensitized solar cells (DSSCs) have rapidly emerged as a promising alternative to conventional silicon photovoltaics

due to their combined benefits of low cost, simple fabrication, environmentally friendly operation, and scalable components [6–9]. The main components of DSSCs are a photoanode consisting of a dye-sensitized semiconductor nanocrystalline thin film (e.g., TiO₂ thin film) deposited on a transparent conducting substrate, a Pt cathode, and a redox-active electrolyte.

A high-performance photoanode is expected to possess a large specific surface area for sufficient dye loading, a direct pathway for fast transport of photo-generated electrons, a pronounced light-scattering effect, and a low charge recombination in the trapping–detrapping site [10–12]. The randomly dispersed TiO₂ nanoparticles provide a large specific surface area for sufficient dye loading, but create numerous grain boundaries which hinder the facile electron transport through the thin film and increase the charge recombination. To overcome this problem, a well-aligned TiO₂ nanostructure arrays such as 1D TiO₂ nanorod arrays [13–15] and TiO₂ nanotube arrays (TNAs) [16–19] have been proposed which can provide

Electronic supplementary material The online version of this article (<https://doi.org/10.1007/s13738-019-01821-0>) contains supplementary material, which is available to authorized users.

✉ Omran Moradlou
moradlou@alzahra.ac.ir

¹ Department of Chemistry, Faculty of Physics & Chemistry, Alzahra University, P.O. Box 1993893973, Tehran, Iran

a direct pathway for electron transport. However, these ideal nanostructures are subjected to a vital shortcoming, i.e., a low surface area when compared with a TiO₂ nanoparticle photoanode of similar thickness, which can lead to insufficient dye absorption and result in lower cell performance. To increase the surface area of nanorod-based photoanodes, various methods including TiCl₄ post-treatment [10] and hydrothermal/chemical etching of TiO₂ nanorods [11, 13] have been reported for the enhancement of the DSSCs performance. The resulted nanostructures are expected to have an enhancement in both light harvesting and electron transport at electrode surface.

However, to increase the surface area, usually the post-etching treatments result in TiO₂ paper-like films detached from the conductive glass substrate [11, 13]. So, to fabricate the photoanode, the detached TiO₂ film should be carefully transferred to a new FTO glass substrate coated with ultra-thin adhesive TiO₂ paste. The partial etching of the nanorod arrays in TiO₂/substrate interface and the existence of nanoparticle-based TiO₂ paste between nanorods and FTO substrate will act as the charge recombination sites in the interfaces and increase the charge transfer resistance.

In this study, we proposed a facile, low cost, and scalable sol-gel method to coat an ultra-thin layer of TiO₂ on FTO substrate as a seed layer for the growth and post-treatment of TiO₂ nanorod arrays. In fact, before the two-step hydrothermal growth and the chemical post-etching treatment of TiO₂ nanorods as well as TiCl₄ post-treatment, the sol-gel method was used for the deposition of about 21 nm of TiO₂ thin film on FTO glass substrate to prepare FTO/TiO₂-sg. This is the first report on the growth of tightly adhered TiO₂ nanorod arrays on FTO by the aid of the sol-gel method. The results showed that the sol-gel-derived seed layer on FTO/TiO₂-sg has a pivotal role for the tight adhesion of TiO₂ nanorod arrays on FTO. So, the resulted 3D-TiO₂ nanorod arrays with high surface area is expected to provide a direct pathway for the electron transport with minimized charge recombination sites in nanorod/FTO interface and decrease in the charge transfer resistance. Finally, DSSCs with iodine- and cobalt complex-based electrolytes were assembled and their characteristics were investigated as well. Based on the results, it was established that a replacement of the photoanode building blocks from commercial TiO₂ nanoparticle to tightly adhered vertically aligned 3D-TiO₂ nanorod arrays enabled a remarkable improvement in the ionic diffusion of cobalt(II/III) tris(2,2'-bipyridine) complexes toward the photoelectrode.

Experimental

Preparation of sol-gel-derived TiO₂ thin films

All the chemicals were of analytic grade and used without further purification. Titanium butoxide and concentrated

hydrochloric acid (HCl, 35%) were purchased from Merck. Sol-gel-derived TiO₂ thin films on FTO (FTO/TiO₂-sg) were prepared via a facile sol-gel method. At first, TiO₂ sol was prepared by mixing titanium *n*-butoxide (1.15 mL) with absolute ethanol (11.50 mL). After 0.5 h stirring, four drops of the concentrated nitric acid were added to the sol as catalyst. The mixed final sol was stirred for 2 h and then agitated for 24 h [20]. The deposition process was performed by using a dip-coating method by dipping the pre-cleaned FTO (1.5 × 1.5 cm²) into the prepared TiO₂ sol for 60 s and pulling it up slowly. The deposited film was dried at 120 °C for 1 h and then annealed in air atmosphere by using the thermal programming with the up ramp rate of $dT/dt = 4$ °C/min from $T_{\text{Initial}} = 25$ °C to $T_{\text{Final}} = 500$ °C, 120 min dwell, and then down ramp rate of 4 °C/min to room temperature. The fabricated TiO₂-coated FTO glass substrate is designated as FTO/TiO₂-sg sample.

Fabrication of FTO/3D-TiO₂-NR photoanode

For the fabrication of 3D-TiO₂ nanorod electrode (FTO/3D-TiO₂-NR), two-step hydrothermal method was used as growth and chemical etching treatment steps. In the hydrothermal nanorod growth step [21], at first, a solution of HCl:H₂O (1:1, *v/v*) was prepared by mixing 15.0 mL of concentrated hydrochloric acid (HCl 35%) with 15.0 mL of ultra-pure deionized water (DI water, Millipore, 18 MΩ) under the magnetic stirring. Then, 0.9 mL of titanium *n*-butoxide was added to the mixture and stirred until a clear solution was obtained. The solution was then transferred to a pre-cleaned 100-mL Teflon-lined stainless steel autoclave, and a FTO/TiO₂-sg film was immersed horizontally into the solution with the coated side facing up and heated to 150 °C for 10 h. After cooling to room temperature, the film was rinsed with DI water and ethanol and dried in air atmosphere. In the hydrothermal chemical etching step [13], a solution of HCl:H₂O was prepared by mixing 11.0 mL of concentrated HCl with 5.0 mL of DI water. The solution was transferred to a 50-mL Teflon-lined stainless steel autoclave, and a prepared TiO₂ nanorod film was immersed vertically into the solution and heated to 150 °C for 12 h. After cooling to room temperature, the obtained 3D-TiO₂ nanorod film was rinsed with DI water and ethanol and dried in air atmosphere. Finally, the electrode was annealed in air atmosphere by using the thermal programming with the up ramp rate of $dT/dt = 4$ °C/min from $T_{\text{Initial}} = 25$ °C to $T_{\text{Final}} = 500$ °C, 120 min dwell, and then, down ramp rate of 4 °C/min to room temperature.

TiCl₄ post-treatment

For TiCl₄ treatment of the FTO/3D-TiO₂-NR electrode, it was immersed in a sealed solution vessel containing

0.04 mol L⁻¹ TiCl₄ (Sigma-Aldrich) and stored in an oven at 70 °C for 30 min. Then, the electrode was rinsed with DI water and ethanol and dried at room temperature. Finally, the electrode was sintered at 460 °C for 30 min.

Composition of the electrolytes

In this study, two types of electrolytes were used in DSSC fabrication: iodine-based and cobalt complex-based electrolytes. The iodine-based electrolyte contained lithium iodide (LiI, 0.10 M), iodine (I₂, 0.010 M), 4-*tert*-butylpyridine (TBP, 0.50 M), butyl methyl imidazolium iodide (BMIMI, 0.60 M), and guanidinium thiocyanate (GuSCN, 0.10 M) in a mixture of acetonitrile (CH₃CN):valeronitrile (*n*-C₄H₉CN) (85:15 v/v) solvent.

For the preparation of cobalt complex-based electrolyte, at first, cobalt(II) tris(2,2'-bipyridine) and cobalt(III) tris(2,2'-bipyridine) complexes were synthesized by a procedure reported elsewhere with modification [8]. Briefly, for the synthesis of [Co(bpy)₃](PF₆)₂ complex, a solution containing 2,2'-bipyridine (0.5154 g of 2,2'-bipyridine(bpy) in a minimum amount of methanol) was added dropwise to an stirred solution of Co²⁺ (0.2379 g of CoCl₂·6H₂O dissolved in 10.0 mL of DI water) and the reaction was allowed to proceed with constant stirring under the reflux conditions for 2 h. An excess amount of ammonium hexafluorophosphate (NH₄PF₆) was added to the solution to precipitate [Co(bpy)₃](PF₆)₂ complex. The obtained solid was filtered, washed with methanol and ethanol, and dried in vacuum oven for 6 h. For the synthesis of [Co(bpy)₃](PF₆)₃ complex, a solution containing 2,2'-bipyridine (0.550 g of 2,2'-bipyridine(bpy) in a minimum amount of methanol) was added dropwise to an stirred solution of Co²⁺ (0.250 g of CoCl₂·6H₂O dissolved in 10.0 mL of DI water) and the mixture was stirred for 5 min. Then, 4.0 mL of H₂O₂ (30%) and 4.0 mL of HCl (30%) were added to the mixture and the reaction was allowed to proceed with constant stirring under the reflux conditions for 3 h. Finally, an excess amount of NH₄PF₆ was added to the solution to precipitate [Co(bpy)₃](PF₆)₃ complex. The obtained solid was filtered, washed with methanol and ethanol, and dried in vacuum oven for 6 h.

The cobalt complex-based electrolyte consisted of 0.20 M [Co(bpy)₃](PF₆)₂ complex, 0.02 M [Co(bpy)₃](PF₆)₃ complex, 0.50 M TBP, and 0.10 M LiClO₄ in acetonitrile.

DSSC assembly

The photovoltaic measurements were taken in a sandwich cell consisting of a dye-sensitized photoanode and a platinum-coated FTO counter electrode. In this study, four types of DSSCs were assembled based on two types of photoanodes and two types of electrolytes. In a typical procedure, to fabricate a DSSC, a dye-sensitized TiO₂-based

electrode (FTO coated with commercial TiO₂ nanoparticles or 3D-TiO₂-NR) was used as photoanode, Pt coated FTO as the counter electrode, and the electrolyte containing I₃⁻/I⁻ or cobalt(II/III) tris(2,2'-bipyridine) complexes as redox couple mediators. To load dye on TiO₂-based photoanodes, they were immersed in an absolute ethanol/acetonitrile (50:50) solution containing 3.0 × 10⁻⁴ mol L⁻¹ N719 for 24 h to adsorb sufficient dye for light harvesting. The dye-loaded samples were then washed with ethanol and acetonitrile to remove the remaining dye. The counter electrode was made by dropcasting of H₂PtCl₆/ethanol solution on FTO glass substrate with the typical size of 1.5 × 1.5 cm² through thermal decomposition at 460 °C for 30 min. DSSC was fabricated in a sandwich configuration by using a dye-loaded photoanode and a counter electrode. The sandwich cells were assembled by sealing the photoanode onto the counter electrode by using a Surlyn (5 × 5 mm²) with the thickness of 60 μm. Finally, a thin layer of electrolyte was introduced into the space between two electrodes as redox couple to evaluate its photovoltaic performance.

Instruments and photovoltaic measurements

The electrochemical measurements were taken using a Galvanostat/Potentiostat Autolab PGSTAT101 instrument. The electrochemical impedance spectroscopy (EIS) of the samples was studied by Autolab PGSTAT 302 N equipped with FRA impedance module. The surface morphology of the fabricated 3D-TiO₂ photoanodes was studied with scanning electron microscopy (VEGA3 TESCAN) and field emission scanning electron microscopy (FE-SEM, MIRA3 TESCAN) equipped with EDAX energy-dispersive X-ray spectrometer (EDS) for inspecting the elemental composition and elemental mapping of the samples. The surface topography of the samples was studied by using Thermo Microscope Autoprobe CP-Research atomic force microscopy (AFM). In order to study the absorption spectra of samples, UV–visible diffuse reflectance spectroscopy (Shimatzu) was used. BaSO₄ was applied as a reflectance standard in DRS experiments. Transmission electron microscopy (TEM, Philips) was used for size and morphology studies. The sunlight simulator (AM 1.5G) was purchased from Sharif Solar Co., Iran. To study the crystal phase of the thin film samples, X-ray diffraction (STOE STADI MP, Germany) with CuK_α radiation (λ = 1.54051 Å) was used by using grazing incidence. To determine the exact thickness of the layer of sol–gel-derived TiO₂ thin film in the nanometer scale, the reflectometry measurements (small-angle X-ray scattering) were carried out with a STOE STADI MP instrument equipped with the STOE thin film attachment and a DECTRIS MYTHENIK silicon strip detector.

Results and discussion

Morphology, surface analysis, and characterizations

To fabricate the 3D-TiO₂ nanorod photoanodes (3D-TiO₂-NR), at first, an ultra-thin layer of TiO₂ film was coated on FTO glass substrate as a seed layer via the sol–gel method to prepare FTO/TiO₂-sg sample. The SEM image of the prepared FTO/TiO₂-sg sample (Fig. 1a) shows that the TiO₂ thin film has been uniformly coated on FTO. Atomic force microscopy (AFM) was also used for the analysis of surface topography of FTO/TiO₂-sg sample. According to the results (Fig. 1b–d), the measured average surface roughness of thin film was 6.2 nm (Fig. 1c) and the mean height of the deposited material on FTO was between 19 and 28 nm (Fig. 1c, d).

As it is clear from the SEM and AFM images, by using the sol–gel method, a very uniform thin film of TiO₂ has been coated on FTO as a seed layer and has a pivotal role for the tightly adhesion of TiO₂ nanorod arrays on FTO. The average crystal seed of TiO₂ was estimated by AFM to be about 160 nm (Fig. 1d).

To investigate the thickness, roughness, and the crystal phase of the coated film, the small-angle X-ray scattering (SAXS) technique was used. As shown in Fig. 2a, the characteristic diffraction peaks of anatase TiO₂ is feasible in pattern, and according to the SAXS results (Fig. 2b), the thickness and roughness of the deposited TiO₂ thin film are 21.3 nm and 2.7 nm, respectively, which confirm the AFM results.

After the preparation of FTO/TiO₂-sg sample, 3D-TiO₂-NR sample was fabricated by two-step hydrothermal process including TiO₂ nanorod growth and the chemical etching steps. Then, the surface morphology of the samples was characterized by FE-SEM and TEM. As shown in Fig. 3a, after the first hydrothermal process, the dominant morphology of TiO₂ nanostructures is nanorod and every individual nanorod is tetragonal in shape with the square top facets. The size of the TiO₂ foursquare side is about 400 nm with about 3–4 μm long. In the chemical etching step (second hydrothermal process), according to the hydrolysis of TiO₂ in acidic media ($\text{TiO}_2 + 4\text{H}^+ \rightarrow \text{Ti}^{4+} + 2\text{H}_2\text{O}$), the core of each square-shaped nanorod is hydrolyzed, and in the top of nanorod, several nanorods with a diameter of about 30 nm are formed (Fig. 3b, c). In fact, when TiO₂ nanorods were immersed in the chemical etching solution containing concentrated hydrochloric acid in a hydrothermal etching process, according to the reaction process, i.e., $\text{TiO}_2 + 4\text{H}^+ \rightarrow \text{Ti}^{4+} + 2\text{H}_2\text{O}$, TiO₂ nanorods begin to dissolve on the relatively unstable crystal faces. According to TEM image analysis of a TiO₂ nanorods (Fig. 3e), after

chemical etching, each nanorod is needle-like in morphology with the average diameter of about 30 nm, confirming the FE-SEM data. In fact, after the second hydrothermal step, two-layer nanostructure is formed with a cubic base and a needle-like nanorods head. When the two-step hydrothermal method for the synthesis of TiO₂ nanorod was proceeded on a bare FTO, after the chemical etching step, TiO₂ nanorod film was detached from the substrate (Fig. 3f), the result that has also been reported in several works [11, 13]. However, by using the FTO/TiO₂-sg as a substrate, after the chemical etching step, a tightly adhered film of vertically aligned 3D-TiO₂ nanorod was obtained (Fig. 3f). It means that the sol–gel-derived ultra-thin film has a crucial role for the tight adhesion of nanorods on FTO substrate during the two-step hydrothermal processes. Based on this finding, it is expected that the synthesized structure brings a remarkable improvement in the electron transfer rate, lack of contact between the redox mediator in the electrolyte and FTO substrate, and decrease in the charge recombination sites in the FTO/TiO₂ interfaces.

After the fabrication and characterization of FTO/3D-TiO₂-NR, it was sensitized with dye N719 by loading dye on photoanode. To confirm dye loading on TiO₂-NR-based photoanode, EDX elemental mapping and diffuse reflectance spectra (DRS) of photoanode and sensitized photoanode were investigated. In the EDX elemental mapping of sensitized photoanode (Fig. 4), the Ru, C, N, and S elements come from dye N719.

The diffuse reflectance spectra (DRS) of photoanode and sensitized photoanode were also investigated (Fig. 5). The UV–Vis absorption spectra of dye N719 show two main absorption peaks at λ_{max} of 388 nm and 535 nm. According to DRS spectra of pristine photoanode, the absorption edge of TiO₂ is about 380 nm, in good agreement with its energy band gap ($E_g = \sim 3.4$ eV). However, DRS spectra of dye-sensitized FTO/3D-TiO₂-NR photoanode show the absorption peak of N719, confirming that the dye was loaded on photoanode.

Photovoltaic measurements of DSSCs

To study the effect of photoanode morphology on the fabricated DSSC performance, various DSSCs with different photoanodes including commercial TiO₂ nanoparticle-coated FTO substrate (FTO/TiO₂-NP) and proposed FTO/3D-TiO₂-NR (3D-TiO₂-NR grown on FTO/TiO₂-sg) photoanodes were assembled. In this stage, a common iodine-based electrolyte was injected into DSSC devices. Then, the photovoltaic performances of these fabricated DSSCs were investigated by measuring the current density (J , mA cm⁻²) versus voltage (V) under the simulated sunlight irradiation (AM 1.5G, 100 mW cm⁻²).

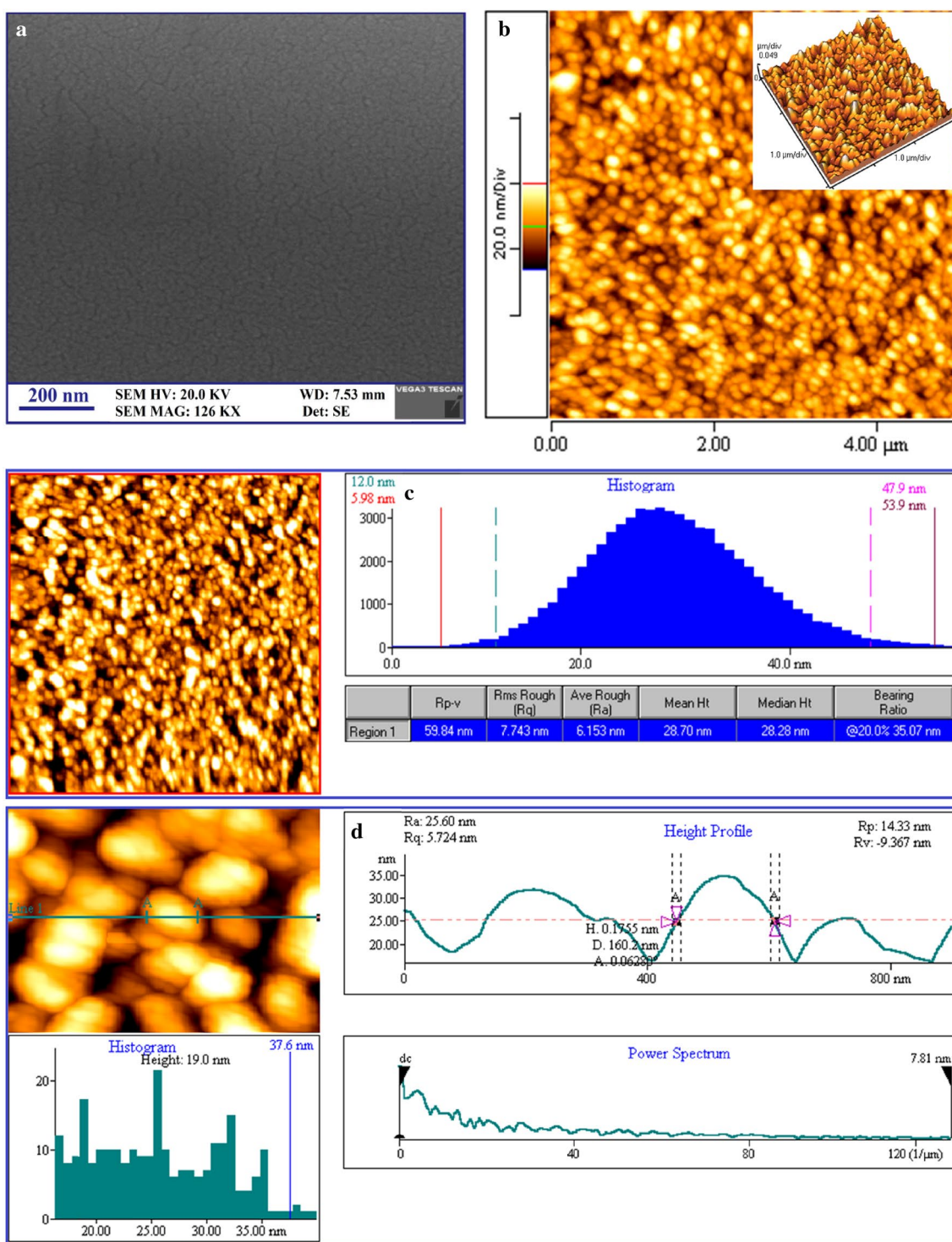


Fig. 1 SEM image (a) and AFM image analyses (b–d) of FTO/TiO₂-sg sample

Figure 6 presents the J - V curves of two DSSCs fabricated by different photoanodes and the injected iodine-based electrolyte. The detailed photovoltaic (PV) parameters including short-circuit photocurrent density (J_{sc}), open-circuit voltage (V_{oc}), fill factor (FF), and efficiency (η) values of DSSCs are

summarized in Table 1. By comparing the results obtained for DSSC-1 and DSSC-2, it is clear that the PV parameters of DSSC-2 which is fabricated by FTO/3D-TiO₂-NR photoanode are comparable with DSSC-1 that is fabricated by FTO/TiO₂-NP photoanode.

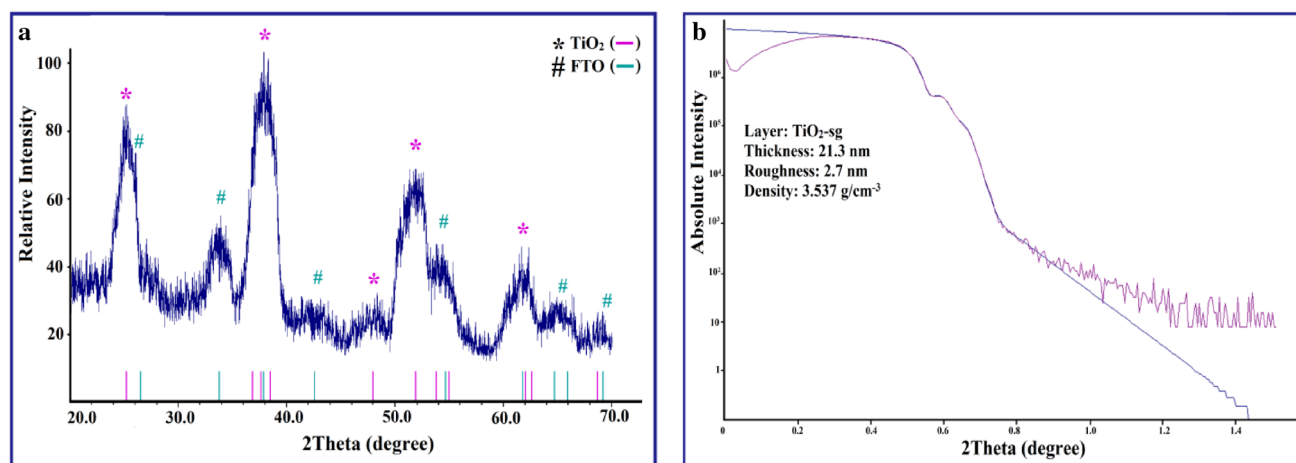


Fig. 2 **a** X-ray diffraction pattern (grazing incidence: 0.3°) of FTO/TiO₂-sg sample. The theoretical reflection positions of TiO₂ (anatase) and SnO₂ (rutile) are indicated by vertical lines. **b** Reflectometry measurement (SAXS) of FTO/TiO₂-sg sample

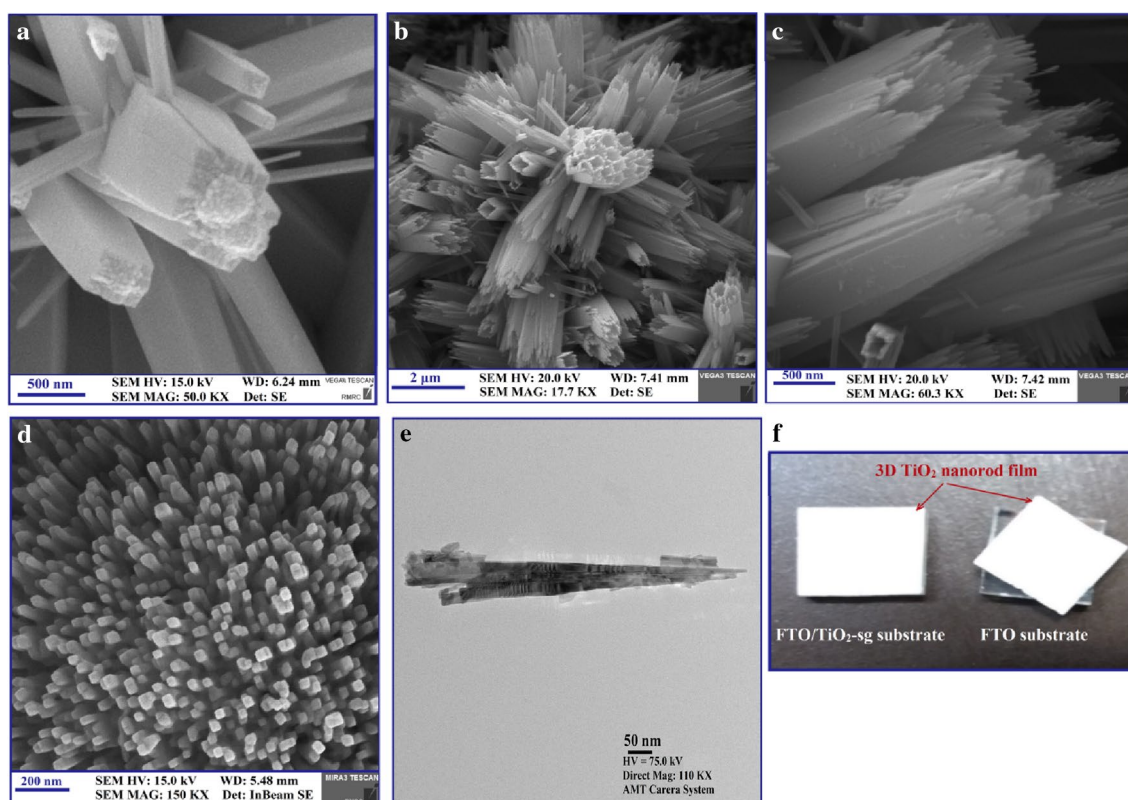


Fig. 3 FE-SEM images of **a** TiO₂ nanorod after the first hydrothermal process (nanorod growth), **b**, **c** 3D-TiO₂ nanorod after the second hydrothermal process (chemical etching), **d** 3D-TiO₂ nanorod after

TiCl₄ post-treatment, **e** TEM image of a needle-like TiO₂ nanorod, and **f** photograph of the resulted FTO/3D-TiO₂-NR photoanode (left) and 3D-TiO₂ film (right)

These results can be mainly attributed to two factors including (1) the efficient photo-harvesting due to the high reflection of 3D-TiO₂-NR compared to the TiO₂ nanoparticles which increases the photon trapping time in the photoanode [8], and (2) direct pathway of the electrons provided

by vertically aligned TiO₂ nanorods [11] which are tightly adhered to FTO substrate. On the other hand, TiO₂ nanoparticles have higher surface area compared to 3D-TiO₂ nanorods which increases dye loading on photoanode and consequently causes higher photo-harvesting. So, based on

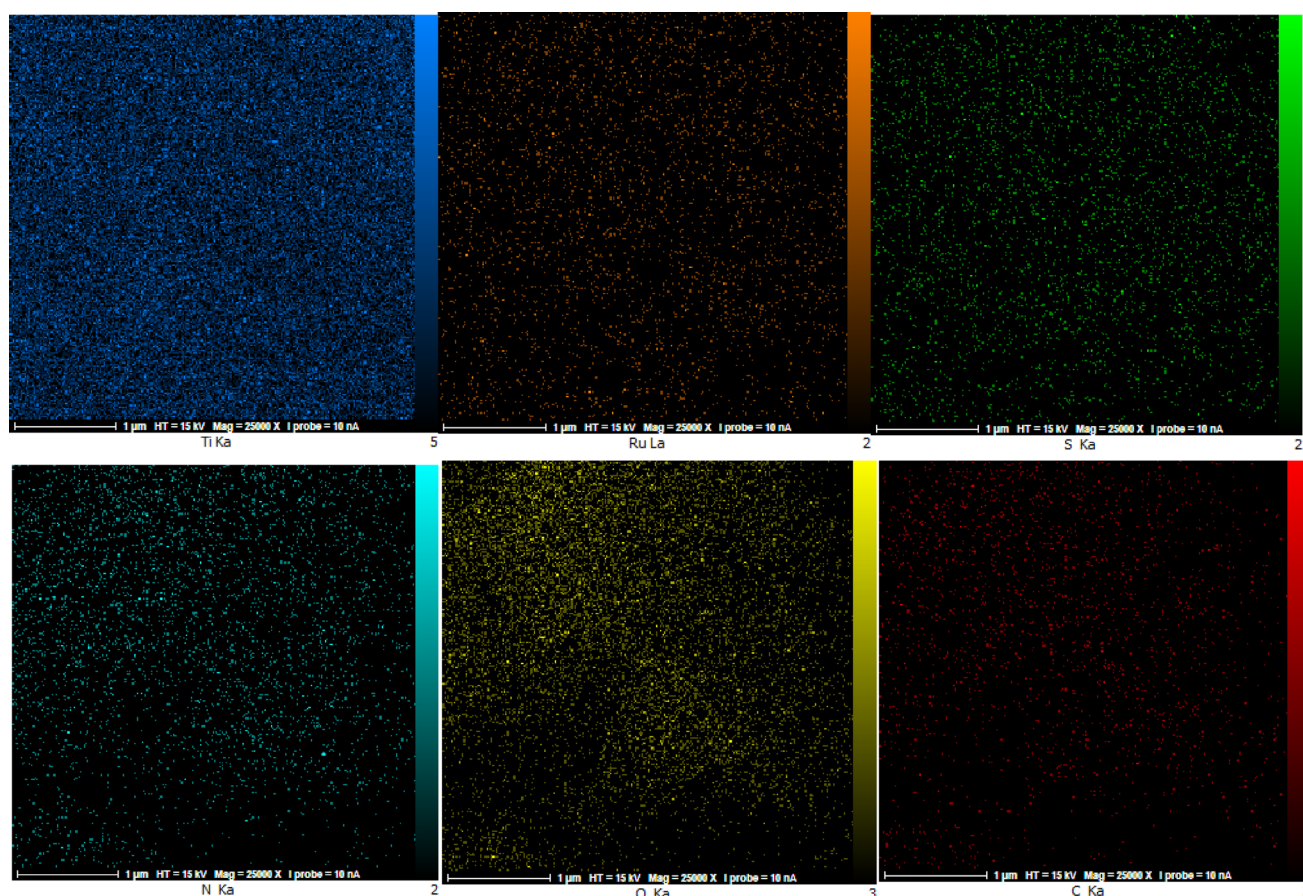


Fig. 4 EDX elemental mapping of N719-sensitized FTO/3D-TiO₂-NR photoanode

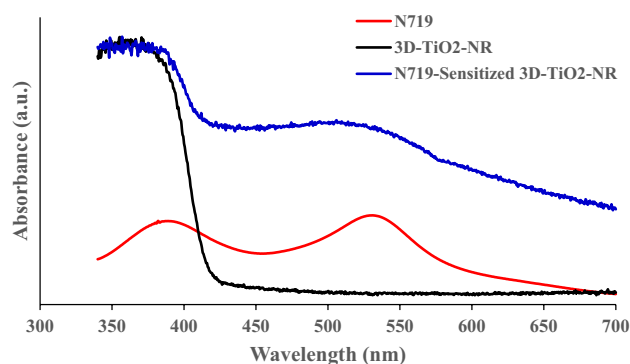


Fig. 5 UV-Vis spectra of N719 and DRS spectra of 3D-TiO₂-NR and dye-sensitized 3D-TiO₂-NR photoanodes

the PV parameters in Table 1, the two factors mentioned above make nanorods to overcome the drawbacks of its lower surface area.

As reported, when the bulky mediators such as cobalt(bpy)₃ complexes are used in the electrolyte, due to their lower diffusion coefficients in the electrolyte, the lower efficiencies for the constructed DSSC are

unavoidable [8, 22–24]. In fact, it seems that the DSSCs with alternative bulky redox shuttles to iodide/triiodide suffer from the limited diffusion of the bulky shuttle to/from the building blocks of photoanodes. However, the drawback could be overcome by change in the morphology of the photoanode building blocks expecting the improvement in the mobility and the ionic diffusion of bulky mediator [23–26]. So, to examine the feasibility of the proposed FTO/3D-TiO₂-NR as photoanode building blocks in DSSCs containing bulky redox mediators, [Co(bpy)₃]^{2+/3+} complexes-based electrolyte was injected into the assembled DSSC devices. Finally, the photovoltaic performances of the fabricated DSSCs were investigated (Fig. 7, Table 2). As it is clear from Fig. 7 and Table 2, all of the PV parameters of DSSC-4 which is fabricated by FTO/3D-TiO₂-NR photoanode have been improved significantly compared to DSSC with common TiO₂ nanoparticles as photoanode building blocks (DSSC-3). Interestingly, η and J_{sc} of DSSCs-4 are improved 2.5 and 2.43 times, respectively. The enhanced efficiency in DSSC-4 is mainly due to the restricted recombination reaction in photoanodes with 3D-TiO₂-NR building blocks [16, 27].

Fig. 6 J - V curves of the fabricated DSSCs with different photoanodes: DSSC-1 with FTO/TiO₂-NP and DSSC-2 with FTO/3D-TiO₂-NR photoanodes. The injected electrolyte was common iodine-based electrolyte and the experiments were performed under AM 1.5G simulated solar irradiation with 100 mW cm⁻²

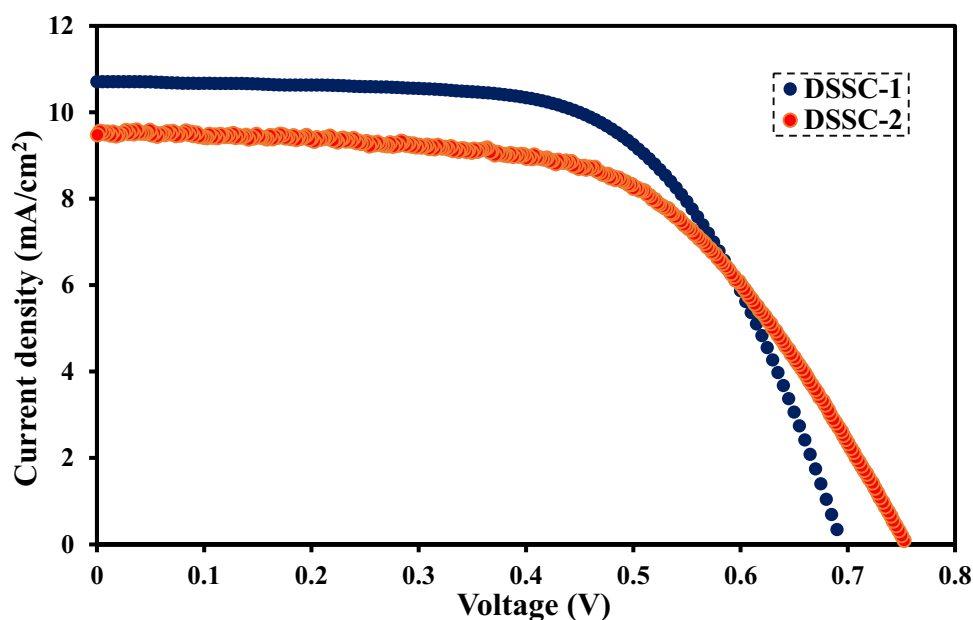


Table 1 Photovoltaic parameters of DSSCs based on different photoanodes with iodine-based electrolytes

DSSC	Photoanode	Mediator	V_{oc} (V)	J_{sc} (mA cm ⁻²)	Fill factor (FF)	Efficiency (η , %)
DSSC-1	FTO/TiO ₂ -NP	I ⁻ /I ₃ ⁻	0.69	10.7	0.63	4.63
DSSC-2	FTO/3D-TiO ₂ -NR	I ⁻ /I ₃ ⁻	0.75	9.6	0.58	4.16

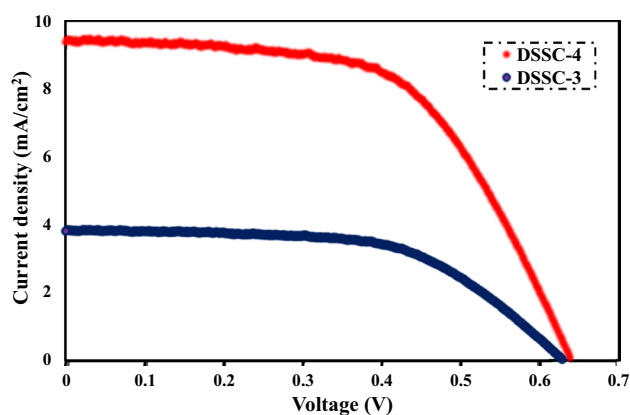


Fig. 7 J - V curve of the fabricated DSSCs with different photoanode: (DSSC-3) FTO/TiO₂-NP, (DSSC-4) FTO/3D-TiO₂-NR. The injected electrolyte was cobalt complex-based electrolyte and the experiments were performed under AM 1.5G simulated solar irradiation with 100 mW cm⁻²

Table 2 Photovoltaic parameters of DSSCs based on different photoanodes with cobalt complex-based electrolytes

DSSC	Photoanode	Mediator	V_{oc} (V)	J_{sc} (mA cm ⁻²)	Fill factor (FF)	Efficiency (η , %)
DSSC-3	FTO/TiO ₂ -NP	[Co(bpy) ₃] ^{2+/3+}	0.62	3.84	0.59	1.4
DSSC-4	FTO/3D-TiO ₂ -NR	[Co(bpy) ₃] ^{2+/3+}	0.64	9.36	0.58	3.5

From the above-mentioned results, it can be concluded that 3D-TiO₂-NR as photoanode building blocks could provide an adequate interspace region in microscale as ionic diffusion freeways allowing a rapid diffusion and storage of the bulky cobalt redox complexes [8, 24]. In fact, the 3D-TiO₂-NR well compensates the slow diffusion of [Co(bpy)₃]^{2+/3+} complexes in the limited space of the foursquare building blocks with the nanorod end. This demonstrates that 3D-TiO₂-NR is an ideal alternative photoanode candidate for the fabrication of DSSCs with bulky mediators for practical applications.

As discussed above, an ultra-thin layer of TiO₂ was coated on FTO substrate as a seed layer for the growth and post-treatment of TiO₂ nanorod arrays. The sol-gel-derived seed layer on FTO/TiO₂-sg had a pivotal role to tightly adhere TiO₂ nanorod arrays on FTO. To confirm, after the photovoltaic studies, the fabricated cell was disassembled and the FE-SEM image and FT-IR spectra of the sensitized

photoanode were taken. As shown in Fig. S1 (Supplementary material), the morphology of 3D-TiO₂ nanorod arrays has not been changed significantly and 3D-TiO₂ nanorods have not been destructed, peeled off, or detached from the surface of FTO substrate. Fourier-transform infrared (FT-IR) spectra of photoanode and dye-sensitized photoanode have also been studied as shown in Fig. S2. The existence of dye on the sensitized photoanode confirms the tight adsorption of dye on the surface of photoanode.

Electrochemical impedance spectroscopy

In order to get more insight into the charge transfer resistance of the fabricated DSSCs, electrochemical impedance spectroscopy (EIS) was used. EIS is a powerful electrochemical technique for studying the resistance of charge transfer as well as the recombination processes. Figures 8 and 9 show the Nyquist plots, their corresponding equivalent circuits, Bode plots, and phase plots of the fabricated DSSCs obtained in open-circuit voltage in the frequency range of 0.1 Hz to 100 kHz under the light illumination conditions.

Generally, the first gap (R_s) is attributed to the sheet resistance of the FTO substrate and the contact resistance between FTO and TiO₂. Also, two semicircles can be expected in EIS, the first semicircle observed in the high-frequency region (left side of the diagram) indicates the charge transfer resistance at the platinum electrode/electrolyte interface (R_{pt}) and

the second semicircle observed in the low-frequency region (right side of the graph) is attributed to the charge transfer resistance (R_{ct}) at the TiO₂/dye/electrolyte interface [13]. Based on the impedance spectra and fitting the data, the values of R_s , R_{ct} , and R_{pt} for the fabricated DSSCs are presented in Table 3.

Figure 8a shows the Nyquist plots for DSSCs fabricated with iodide/triiodide mediator in solution. As it is clear, the charge transfer resistances of R_s , R_{ct} , and R_{pt} for DSSC-2 with FTO/3D-TiO₂-NR photoanode building blocks are lower than that of DSSC-1 indicating the increase in the electron transfer rate as well as the easier diffusion of redox couple in the electrolyte/electrodes interfaces. For DSSCs fabricated with [Co(bpy)₃]^{2+/3+} complex shuttles, as shown in Fig. 9a, the lower charge transfer resistances for DSSC-4 indicate the suitable structural matching of photoanode building block and the lower diffusion coefficient of bulky [Co(bpy)₃]^{2+/3+} complexes. In fact, the nanorod structure of 3D-TiO₂-NR provides an adequate interspace region in microscale as ionic diffusion freeways to easier diffusion of the redox shuttles. Therefore, it can be concluded that employing the nanorod structure instead of the nanoparticle as photoanode building block would greatly overcome the diffusion problem of the bulky redox shuttles.

The overall charge transfer scheme for the DSSCs is shown in Fig. 10. When the incident photon is absorbed by N719 as photosensitizer, the excited electrons from LUMO

Fig. 8 Nyquist plot (a), Bode plot (b), and the phase plot (c) of DSSCs fabricated with different photoanodes including DSSC-1 (TiO₂-NP) and DSSC-2 (TiO₂-3D-NR). The injected electrolyte in the cells contained iodide/triiodide redox mediator

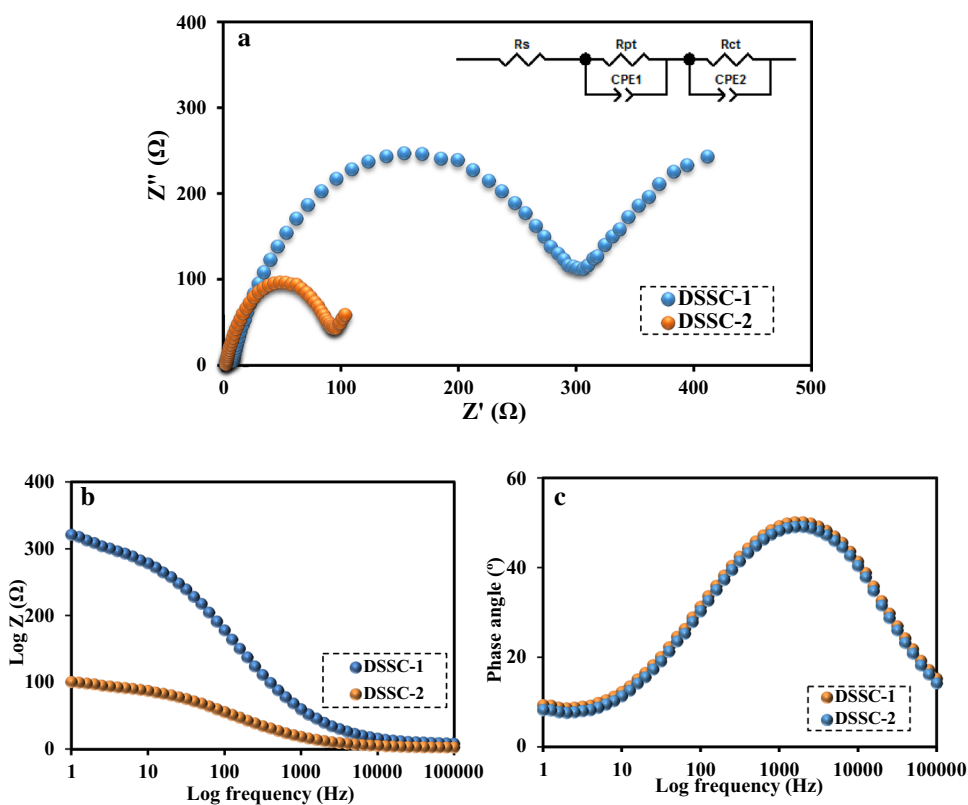


Fig. 9 Nyquist plot (a), Bode plot (b), and the phase plot (c) of DSSCs fabricated with different photoanodes including DSSC-3 (TiO₂-NP) and DSSC-4 (TiO₂-3D-NR). The injected electrolyte in the cells contained redox shuttle (Co(bpy)₃)^{2+/3+} complexes

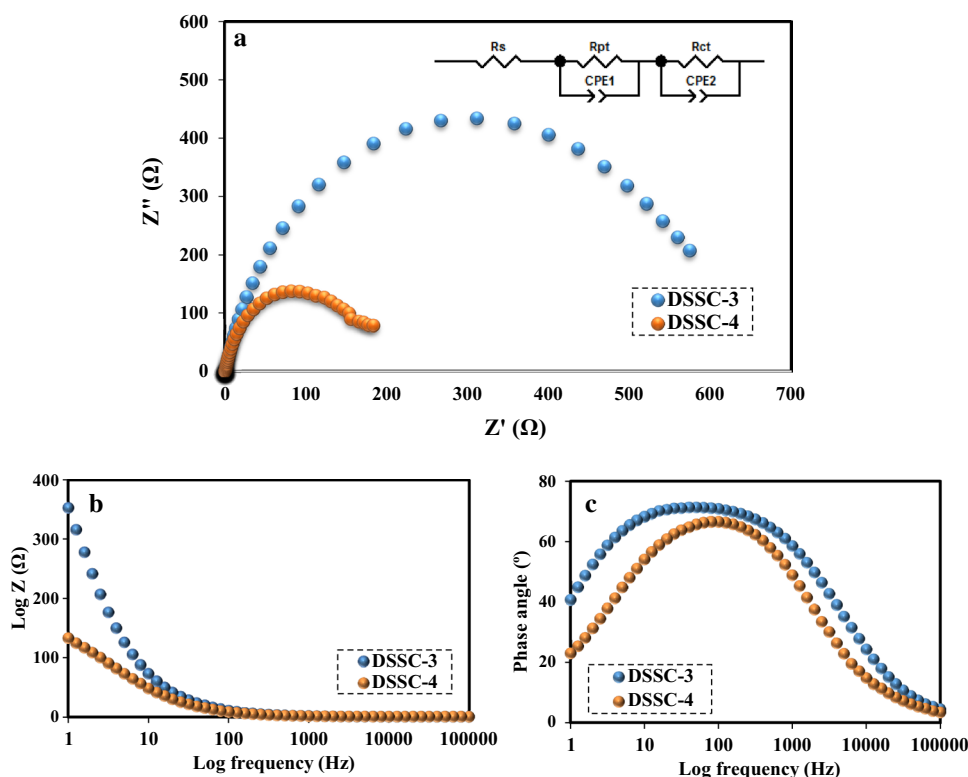


Table 3 Details of the resistance values of the fabricated DSSCs

DSSC	Photoanode	Mediator	R_s (Ω)	R_{pt} (Ω)	R_{ct} (Ω)
DSSC-1	FTO/TiO ₂ -NP	I ⁻ /I ₃ ⁻	7.0	151	421
DSSC-2	FTO/3D-TiO ₂ -NR	I ⁻ /I ₃ ⁻	2.5	47	71
DSSC-3	FTO/TiO ₂ -NP	[Co(bpy) ₃] ^{2+/3+}	0.5	289	–
DSSC-4	FTO/3D-TiO ₂ -NR	[Co(bpy) ₃] ^{2+/3+}	0.7	79	1616

of N719 are injected into the conduction band of TiO₂ and finally flow through the external circuit to the counter electrode FTO/Pt. The oxidized photosensitizer accepts electrons from the redox mediator in the electrolyte, [Co(bpy)₃]^{2+/3+} or I₃⁻/I⁻ couple, leading to regeneration of dye. Finally, the oxidized redox mediator diffuses toward the counter electrode and then is reduced.

Conclusions

In this study, a facile, low cost, and scalable sol–gel method was proposed to coat an ultra-thin layer of TiO₂ on FTO substrate as a seed layer for the growth of 3D-TiO₂ nanorod arrays. The sol–gel-derived seed layer on FTO/TiO₂-sg had a pivotal role for the tightly adhesion of TiO₂ nanorod arrays grown on FTO and the resulted 3D-TiO₂-NR provided

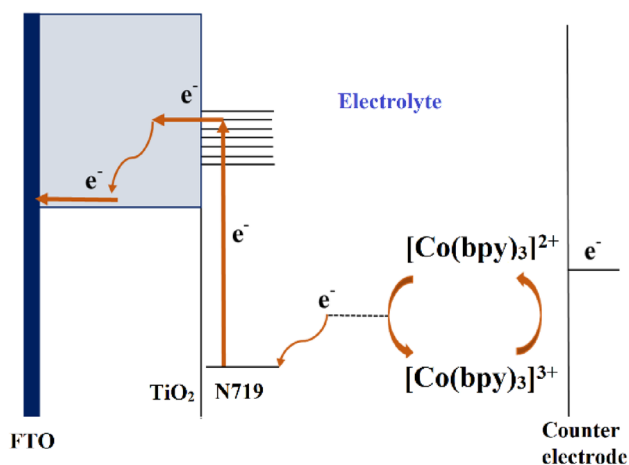


Fig. 10 Overall charge transfer scheme. Charge transfer scheme for the DSSCs fabricated with [Co(bpy)₃]^{2+/3+}-based electrolyte

a direct pathway for the electron transfer in nanorod/FTO interface. The 3D-TiO₂-NR nanostructure was used as photoanode building block in the fabrication of DSSCs based on iodide/triiodide as well as [Co(bpy)₃]^{2+/3+} redox shuttle, and the photovoltaic parameters of fabricated DSSCs were compared with DSSCs with TiO₂-NP photoanode. Due to the rapid diffusion of redox couple, especially [Co(bpy)₃]^{2+/3+} shuttles in 3D-TiO₂-NR structure, the photovoltaic parameters were improved significantly in DSSC-4. The rapid diffusion of cobalt redox couple in 3D-TiO₂-NR structure leads

to the remarkable reduction in the charge transfer resistance in DSSC-4.

Acknowledgements The authors would like to thank Research Council of Alzahra University for financial support (Grant No. 1397). A special thanks go to Dr. Simon Welzmler and Dr. Sascha Correll (STOE Company, Germany) for their small-angle X-ray scattering (SAXS) measurements and valuable discussions.

References

1. M. Abrari, M. Ahmadi, M. Ghanaatshoar, H.R. Moazami, S.S.H. Davarani, *J. Alloys Compd.* **784**, 1036 (2019)
2. W. Liang, K. Fan, Y. Luan, Z. Tan, M. Al-Mamun, Y. Wang, P. Liu, H. Zhao, *J. Alloys Compd.* **772**, 80 (2019)
3. Y. Rui, Y. Li, Q. Zhang, H. Wang, *CrystEngComm* **15**, 1651 (2013)
4. G. Liu, J. Xu, K. Wang, *Mater. Today Energy* **10**, 368 (2018)
5. O. Moradlou, Z. Rabiei, A. Banazadeh, J. Warzywoda, M. Zirak, *Appl. Catal. B: Environ.* **227**, 178 (2018)
6. Z.J. Chermahini, A.N. Chermahini, H.A. Dabbagh, B. Rezaei, N. Irannejad, *J. Iran. Chem. Soc.* **14**, 1549–1556 (2017)
7. A. Hagfeldt, G. Boschloo, L. Sun, L. Kloo, H. Pettersson, *Chem. Rev.* **110**, 6595 (2010)
8. X.L. Zhang, W. Huang, A. Gu, W. Xiang, F. Huang, Z.X. Guo, Y.-B. Cheng, L. Spiccia, *J. Mater. Chem. C* **5**, 4875 (2017)
9. P. Naik, R. Su, D.D. Babu, A. El-Shafei, A.V. Adhikari, *J. Iran. Chem. Soc.* **14**, 2457–2466 (2017)
10. M.A. Hossain, S. Oh, S. Lim, *J. Ind. Eng. Chem.* **51**, 122 (2017)
11. B. Wang, J. Wan, Q. Liu, J. Zhang, H. Wang, *RSC Adv.* **5**, 82968 (2015)
12. K. Zhao, X. Zhang, M. Wang, W. Zhang, X. Li, H. Wang, L. Li, *J. Alloys Compd.* **786**, 50–55 (2019)
13. H. Wang, B. Wang, J. Yu, Y. Hu, C. Xia, J. Zhang, R. Liu, *Sci. Rep.* **5**, 9305 (2015)
14. Y.-Y. Li, J.-G. Wang, H.-H. Sun, B. Wei, *ACS Appl. Mater. Interfaces* **10**, 11580 (2018)
15. T.S. Girisun, C. Jeganathan, N. Pavithra, S. Anandan, *Nanotechnology* **29**, 085605 (2018)
16. L.-L. Li, C.-Y. Tsai, H.-P. Wu, C.-C. Chen, E.W.-G. Diau, *J. Mater. Chem.* **20**, 2753 (2010)
17. B. Rezaei, I. Mohammadi, A.A. Ensafi, M.M. Momeni, *Electrochim. Acta* **247**, 410 (2017)
18. Q. Sun, Y. Hong, T. Zang, Q. Liu, L. Yu, L. Dong, *J. Electrochem. Soc.* **165**, H3069 (2018)
19. S. So, A. Kriesch, U. Peschel, P. Schmuki, *J. Mater. Chem. A* **3**, 12603 (2015)
20. N. Naseri, M. Yousefi, O. Moradlou, A. Moshfegh, *Phys. Chem. Chem. Phys.* **13**, 4239 (2011)
21. H. Wang, Y. Bai, H. Zhang, Z. Zhang, J. Li, L. Guo, *J. Phys. Chem. C* **114**, 16451 (2010)
22. J. Wu, Z. Lan, J. Lin, M. Huang, Y. Huang, L. Fan, G. Luo, *Chem. Rev.* **115**, 2136 (2015)
23. A. Colombo, C. Dragonetti, M. Magni, D. Roberto, F. Demartin, S. Caramori, C.A. Bignozzi, *ACS Appl. Mater. Interfaces* **6**, 13945 (2014)
24. L. Xu, C. Xin, C. Li, W. Wu, J. Hua, W. Zhu, *Sol. Energy* **169**, 450 (2018)
25. E.J. Crossland, N. Noel, V. Sivaram, T. Leijtens, J.A. Alexander-Webber, H.J. Snaith, *Nature* **495**, 215 (2013)
26. C. Dong, W. Xiang, F. Huang, D. Fu, W. Huang, U. Bach, Y.-B. Cheng, X. Li, L. Spiccia, *Nanoscale* **6**, 3704 (2014)
27. W. Yang, P. Yang, Q. Tang, *Mater. Lett.* **180**, 228 (2016)